JOURNAL OF MATERIALS SCIENCE 16 (1981) 355–366

Crystal growth of manganese silicide, $MnSi_{\sim 1.73}$ and semiconducting properties of $Mn_{15}Si_{26}$

I. KAWASUMI,* M. SAKATA
Department of Instrumentation, Faculty of Engineering, Keio University, 3-14-1, Hiyoshi, Kohoku-ku, Yokohama 223, Japan

I. NISHIDA, K. MASUMOTO
National Research Institute for Metals, 2-3-12, Nakameguro, Meguro-ku, Tokyo 153, Japan

Boules of the most silicon-rich silicide of manganese, $MnSi_{\sim 1.73}$, were grown by the Bridgman method in the composition range from 62.96 to 63.64 at % Si. There are plate-like MnSi precipitates parallel to the *c*-plane of $Mn_{15}Si_{26}$ matrix in all boules except at their upper and lower ends. The amount of the MnSi precipitates was about 2 vol %. Measurements of electrical resistivity, Hall coefficient, and thermoelectric power of the boules were made in the temperature range from 77 to 1200 K. Thermoelectronic properties of $Mn_{15}Si_{26}$ were estimated on the basis of the distribution state of MnSi precipitates in the boule by assuming that metallic MnSi and semiconducting $Mn_{15}Si_{26}$ alternately crystallized in lamellae. Although the resistivities and thermoelectric powers measured in the *c*- and *a*-axis directions of $Mn_{15}Si_{26}$ showed anisotropy, the former were proportional to exp (4073/*T*) in the intrinsic region in both directions. The Hall coefficients showed isotropy over the whole temperature range. The degenerate hole-concentration of $Mn_{15}Si_{26}$ was determined to be 2.1×10^{27} m^{-3}. Hall mobilities of $Mn_{15}Si_{26}$ in both the *c*- and *a*-axis directions obey a $T^{-3/2}$-law above 600 K. The Hall coefficient calculated from this relationship was in good agreement with the one found for $Mn_{15}Si_{26}$ in the intrinsic region. The effective-hole masses of $Mn_{15}Si_{26}$ along the *c*- and *a*-axis were found to be, respectively, 15 and 11 times larger than those of a free electron. Assuming that acoustic lattice scattering is dominant and that carriers obey Fermi–Dirac statistics, the temperature dependence of the calculated thermoelectric power was in reasonable agreement with the one estimated for $Mn_{15}Si_{26}$ in the temperature range from 400 to 1200 K.

1. Introduction

The most silicon-rich silicide of manganese is interesting as a thermoelectric conversion element for use in higher temperature atmospheres because of its refractory [1–3] and semiconducting properties [4–6]. This silicide was first shown to be stoichiometric $MnSi_2$ by Boren [7] and Hansen [8]. Since their work, many investigators [9–12] have examined Mn–Si alloys with silicon contents between 60.6 and 70.5 at % by means of metallographic, X-ray and thermal analysis, and thermoelectric measurements to confirm this composition. They have concluded that the most silicon-rich silicide of manganese is not the stoichiometric $MnSi_2$ but is $MnSi_{\sim 1.73}$ with silicon composition in the range from 63.0 to 63.6 at %.

The crystal structure of $MnSi_{\sim 1.73}$, which was deduced from the $TiSi_2$-structure [13], was first reported by Schwomma *et al.* [14]. Mn-atoms occupy Ti-sites in the structure and form a sub-

*Present address: Kyorin University, School of Health Science, 476 Miyashita-cho, Hachioji-city, Tokyo 192, Japan.

0022–2461/81/020355–12$03.20/0

lattice with tetragonal symmetry, while Si-atoms are arranged in a dumb-bell-like configuration in the c-axis direction of the sub-lattice. The unit cell is composed of 11 sub-lattices with 44 manganese and 76 silicon atoms. The silicide is represented by $Mn_{11}Si_{19}$ ($MnSi_{1.727}$) with lattice parameters of $a = 0.5515$ nm and $c = 4.8136$ nm. Melt-grown single-crystals with compositions near $MnSi_{\sim 1.73}$ were analysed by X-ray techniques, showing $Mn_{26}Si_{45}$ [15], $Mn_{15}Si_{26}$ [16], $Mn_{27}Si_{47}$ [17], and Mn_4Si_7 [18], in the composition range from 63.38 to 63.64 at% Si. Ivanova *et al.* [19] and Abrikosov *et al.* [20], however, reported the presence of striations perpendicular to the c-axis in a $MnSi_{1.72}$ boule grown by the Czochralski method. Moreover, Levinson [21], Kojima *et al.* [22, 23], and Kawasumi *et al.* [24] have confirmed the plate-like MnSi precipitates along the c-plane of the matrix in a $MnSi_{\sim 1.73}$ boule grown by the Bridgman method.

There are many different reports of the thermoelectric properties of the most silicon-rich silicide of manganese because of the complexities of the silicon composition and the crystal structure. The electrical resistivity, ρ, thermoelectric power, α, and energy gap, E_g of this silicide are 9.4–62 $\mu\Omega$ m, 81–180 μV K^{-1}, and 0.0064–0.0128 aJ (0.40–0.80 eV), respectively [9, 10, 12, 19–21, 25–36]. But, for the Mn–Si alloys with compositions between 60.6 and 70.5 at% Si, ρ, α, and the figure of merit, Z, at room temperature have maximum values of 3.0×10^{-5} Ω m, 120 μV K^{-1}, and 3.0×10^{-5} K^{-1} for silicon compositions near 63.4 at% ($MnSi_{\sim 1.73}$), respectively [9, 12, 24, 26]. Moreover, the ρ and α values for the boules grown by the Czochralski [19–20, 27] and/or Bridgman methods [21] show anisotropy between the c- and a-axis directions at room temperature. ρ and α values measured along the c-axis of a $MnSi_{\sim 1.73}$ boule are about 5 and 1.5 times as large, respectively, as those measured along the a-axis. The temperature dependences of ρ and α of $MnSi_{1.72}$ boules are already reported by Ivanova *et al.* [19] and by Abrikosov *et al.* [20], but the Hall coefficient has not been measured in detail.

On the other hand, the thermoelectric properties of semiconducting $MnSi_{\sim 1.73}$ are considered to be influenced by the metallic MnSi [36, 37], which precipitates along the c-plane of $MnSi_{\sim 1.73}$. In fact, Levinson [21] has reported that the metallic MnSi precipitate degrades the figure of merit, Z, of $MnSi_{\sim 1.73}$. In this work plate-like MnSi precipitates were found along the c-plane of the $Mn_{15}Si_{26}$ matrix in the boules grown by the Bridgman method in the silicon composition range from 63.17 to 63.64 at% [24].

In this study, $MnSi_{\sim 1.73}$ boules were grown by the Bridgman method in the composition range between 62.96 and 63.64 at% Si, and the properties of the MnSi precipitates were examined by metallographic, X-ray, and electron microprobe X-ray analyser (EMX) techniques. Also, the electrical resistivity, thermoelectric power, and Hall coefficient of the boules were measured for a wide range of temperatures. The thermoelectric properties of $Mn_{15}Si_{26}$ were estimated from the two-band model by assuming that metallic MnSi and semiconducting $Mn_{15}Si_{26}$ were alternately formed in lamellae. To clearly determine the conduction mechanism of $Mn_{15}Si_{26}$, the carrier concentration and the thermoelectric power were analysed on the simple two-band model and were compared with those estimated for $Mn_{15}Si_{26}$.

2. Experimental procedure

2.1. Crystal growth

Manganese flakes of purity 99.999% and n-type silicon single-crystal chips of a resistivity about 1 Ω m at room-temperature were used as raw materials to grow $MnSi_{\sim 1.73}$ boules. These materials were weighed-out in the atomic ratios Si/Mn from 1.70 to 1.75 and then arc-melted directly in an argon atmosphere. The alloys obtained were rich in silicon compared with the desired compositions, because of vaporization of Mn-atoms [23]. Because of this, the MnSi single-crystals were first grown by the Bridgman method and then used as a starting material to grow $MnSi_{\sim 1.73}$ boules.

MnSi alloy was prepared by arc-melting manganese flakes and silicon single-crystal chips, which were weighed in the atomic ratio of Si/Mn = 1.00, in an argon atmosphere. The alloy obtained was crushed in an agate mortar into particles of about 1 mm in size and then put into a quartz tube with a pointed bottom, which was protected by a recrystallized Al_2O_3 crucible and Al_2O_3 powder of about 0.5 mm particle size. A MnSi boule was then grown in a Bridgman furnace in an argon atmosphere. The starting temperature, temperature gradient in the vicinity of the liquid–solid phase boundary, and growth rate were 1573 K, 2000 K m^{-1} and 2.22 μm sec^{-1}, respectively. The size of the MnSi boule obtained was about 15 mm in diameter and 150 mm in length. From X-ray

and chemical analysis of the boule, it was found that the silicon content was 50.9(8) at %, which corresponds to a composition of $MnSi_{1.04}$.

Starting with the mixed powder, composed of MnSi and silicon single-crystals of 1 to 2 mm particle size, as mentioned above, $MnSi_{\sim 1.73}$ boules with Si/Mn atomic ratios of 1.70, 1.72 and 1.75 were grown in the Bridgman furnace. The Bridgman furnace was first kept at 1573 K for 3.6 ksec in order to melt the mixed powder completely in the quartz tube. Then the temperature of the furnace was reduced to 1473 K, and the $MnSi_{\sim 1.73}$ boules were grown at a rate of 2.22 $\mu m\,sec^{-1}$. Each boule, about 15 mm in diameter and about 35 mm in length, was subjected to annealing at 1373 K for 720 ksec in an evacuated quartz tube.

The boules were identified by an X-ray powder diffractometer (Rigaku Denki Co. Ltd, RU-3SL), and lattice parameters of the matrix were calculated by an LC-3 program system [37], using all the back diffraction lines of $CrK\alpha_1$ and $K\alpha_2$. The amounts of Mn and Si in the boule were determined by chemical analysis and EMX.

2.2. Measurements of thermoelectric properties

In order to measure the thermoelectric properties of $MnSi_{\sim 1.73}$ boules under the conditions in which the electric field is parallel to the *a*- and *c*-axis directions of the matrix, respectively, a pair of parallelopiped samples of $0.3 \times 4 \times 8\,mm^3$ size were cut from the same boule using a wire saw. Their surfaces were lapped with Al_2O_3 powder of particle size 0.3 μm before metallographic observation. The orientations of crystal axes, electric current, and applied magnetic field for the sample are shown in Fig. 1. The electrical resistivity and Hall coefficient were measured by the d.c. method generally used [39]. Hall coefficient measurements were made in a magnetic field of 0.5 T. Thermoelectric power was measured by the method used by Sakata *et al.* [40]. While varying the temperature difference, ΔT, between the two edges of the sample in the range from 0.5 to 3.0 K, the thermoelectromotive force, E, and ΔT were measured using digital voltmeters. Thermoelectric power was determined from the gradient of the $E-\Delta T$ function and is represented as an absolute value.

3. Experimental results

3.1. Characterization of $MnSi_{\sim 1.73}$ boules

Results of X-ray identification and chemical analysis for $MnSi_{\sim 1.73}$ boules with Si/Mn atomic ratios of 1.70, 1.72 and 1.75 are listed in Table I. The lattice parameters of the $Mn_{15}Si_{26}$ matrix are also included. The (1 0 0) plane of the boule

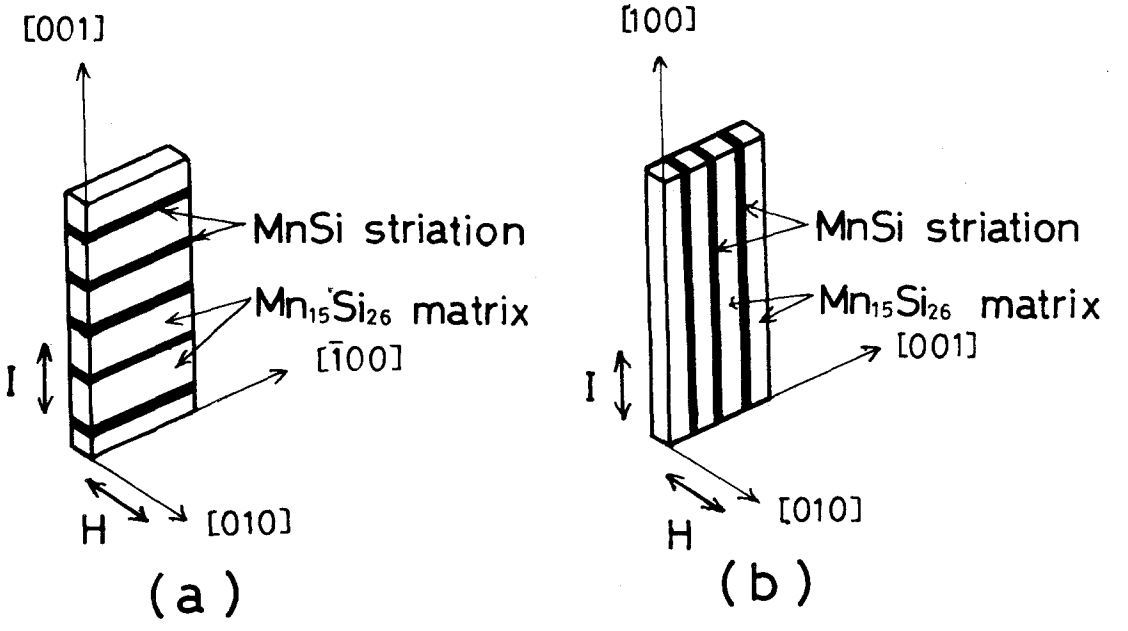

Figure 1 Relationships of the crystal axes directions, the electric current, I, and the applied magnetic field, H, for samples cut from the same $MnSi_{\sim 1.73}$ boule. (a) to measure the values along the [0 0 1] direction; (b) to measure the values along the [1 0 0] direction.

TABLE I Results of X-ray identification and chemical analysis of $MnSi_{\sim 1.73}$ boules with nominal atomic ratios of silicon to manganese (Si/Mn)

Kinds of boule	Identified phases	Compositions (at %)		Si/Mn atomic ratio	Lattice parameters (nm)	
		Mn	Si		*a*	*c*
Si/Mn atomic ratio of 1.70						
upper end	$Mn_{15}Si_{26}$ + MnSi (vw)*	36.8(5)	63.1(5)	1.71(4)	0.552(6)	6.54(1)
middle	$Mn_{15}Si_{26}$ + MnSi (vw)	36.8(3)	63.1(7)	1.71(5)	0.552(3)	6.54(5)
lower end	$Mn_{15}Si_{26}$(w)* + MnSi	47.6(2)	52.3(8)	1.10(0)	–	–
Si/Mn atomic ratio of 1.72						
upper end	$Mn_{15}Si_{26}$ + MnSi (vw)	36.8(3)	63.1(7)	1.71(5)	0.552(5)	6.54(2)
middle	$Mn_{15}Si_{26}$ + MnSi (vw)	36.8(2)	63.1(8)	1.71(5)	0.552(6)	6.54(1)
lower end	$Mn_{15}Si_{26}$ + MnSi (vw)	36.8(5)	63.1(5)	1.71(4)	0.552(4)	6.54(3)
Si/Mn atomic ratio of 1.75						
upper end	$Mn_{15}Si_{26}$ + Si + MnSi (vw)	–	–	–	0.552(4)	6.54(3)
middle	$Mn_{15}Si_{26}$ + MnSi (vw)	36.8(3)	63.1(7)	1.71(5)	0.552(3)	6.54(1)
lower end	$Mn_{15}Si_{26}$ + MnSi (vw)	36.8(5)	63.1(5)	1.71(4)	0.552(5)	6.54(2)

*w and vw are weak and very weak diffraction intensities, respectively.

with Si/Mn atomic ratio of 1.72 is shown in Fig. 2 as a typical polarized photograph. As can be seen in Table I, the amounts of Mn and Si in the three portions of the upper and lower ends and the middle of the boule with Si/Mn atomic ratio of 1.72 are in good agreement with one another within chemical accuracy. From the results of X-ray analysis, it was determined that the boule was of two phases, composed of $Mn_{15}Si_{26}$ matrix [16] and MnSi striation [7]. The main diffraction lines of $Mn_{15}Si_{26}$ and the very weak ones of MnSi were identified for all the portions of the boules. In the boule with Si/Mn atomic ratio of 1.70, MnSi crystal was grown up to about ten millimeters from the lower end. In the boule with Si/Mn atomic ratio of 1.75, free Si was formed down to a few millimeters from the upper end. These results are quite consistent with the characterization of $MnSi_{2-x}$ boules reported by Kawasumi *et al.* [23]. As shown in Table I, the Si content and the lattice parameters of $Mn_{15}Si_{26}$ are in good agreement with one another for the middle portions of the three boules.

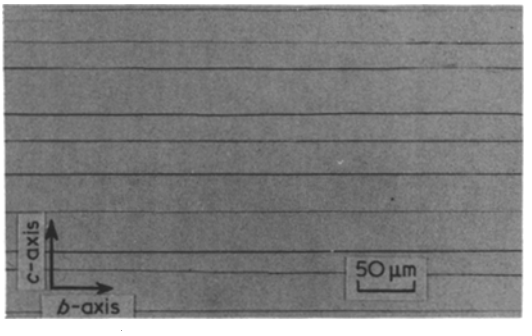

Figure 2 The (1 0 0) plane of the boule with Si/Mn atomic ratio of 1.72. The black lines are the MnSi plate-like precipitates.

From the Laue diffraction photograph and from metallographic observation, the striations seen in Fig. 2 were observed, not in the *c*-plane, but in the planes parallel to the *c*-axis. This shows that these striations are plate-like precipitates parallel to the *c*-plane of the $Mn_{15}Si_{26}$ matrix. The mean sizes of the striations are 0.6 μm in width and 175 μm in length, and the mean distance between them is 30 μm on the (1 0 0) plane of the boule. Fig. 3 shows the X-ray intensities produced from Mn and Si, obtained by EMX line-scanning perpendicular to the striations in the (1 0 0) plane of the boule with Si/Mn atomic ratio of 1.72. As shown in Fig. 3, the intensities produced by Mn and Si in the striations are in good agreement with those produced for the MnSi single crystal used as the standard sample (Fig. 3b). From the results of the quantitative EMX analysis, the amounts of Si were 50.5 at % for the striations and 63.2 at % for the matrix corresponding to MnSi and $Mn_{15}Si_{26}$ ($MnSi_{1.733}$), respectively. Therefore, it was found that the black striations in Fig. 2 are the plate-like MnSi and that the volume-ratio of MnSi striations to the $Mn_{15}Si_{26}$ matrix, *f*, is 0.02, which corresponds to the value obtained from the magnetic measurement [21]. In fact, using $f = 0.02$, the calculated Si-content of the boule is 63.1(7) at % ($MnSi_{1.715}$) and so is in reasonable agreement with the result obtained by chemical analysis.

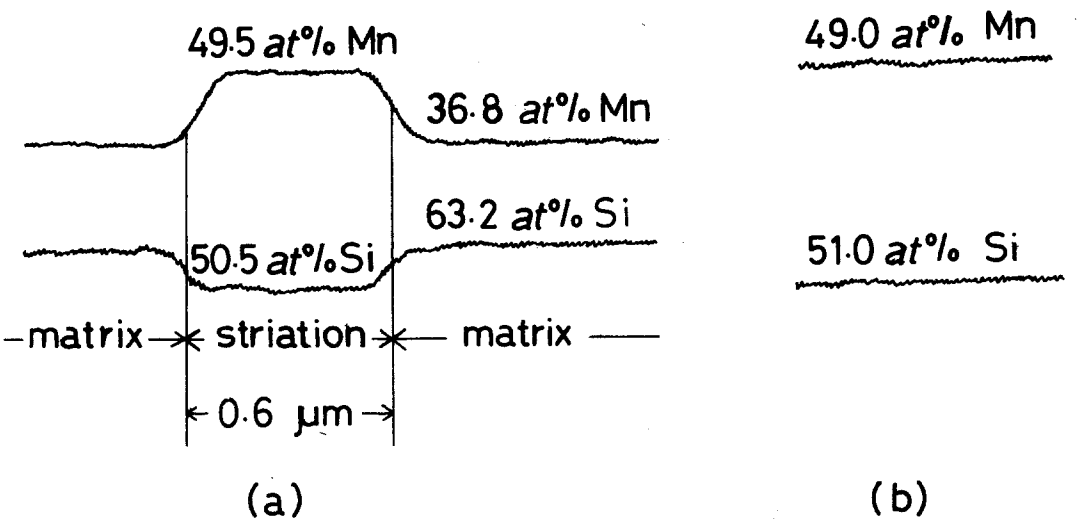

Figure 3 X-ray intensities of Mn and Si obtained by EMX analysis for the boule with Si/Mn atomic ratio of 1.72 and for a MnSi single-crystal. (a) the boule with Si/Mn atomic ratio of 1.72; (b) a MnSi single-crystal as the standard sample.

3.2. Thermoelectric properties of $MnSi_{\sim 1.73}$ boules

Table II shows electrical resistivity, ρ, thermoelectric power, α, and the Hall coefficient, R, at room temperature for the samples, which were cut from the middle portion of each boule in Table I. No great difference was found in the values of ρ, α, and R, shown in Table II, for the three boules and their values were found to be independent of the compositions of starting materials. Resistivity and thermoelectric power ratios of the c- to a-axis directions, ρ_c/ρ_a and α_c/α_a, were about 5.1 and 1.3, respectively, and are in good agreement with those reported by Ivanova *et al.* [19] and Abrikosov *et al.* [20]. On the contrary, the Hall coefficient ratio of the c- to a-axis directions, R_c/R_a, was found to be less than unity, about 0.81. Fig. 4 shows the relationships between temperature and resistivities in the c- and a-axis directions of the boule with Si/Mn atomic ratios of 1.72 (open points). The temperature variation of the boule resistivity in the c-axis direction, ρ_c, is similar to that found for the a-axis, ρ_a, over the whole temperature range (broken lines in Fig. 4a and b). However, the ratio ρ_c/ρ_a increases with decreasing temperature because the change in ρ_c is smaller than the change in ρ_a for the lower temperature range. The values of ρ_c/ρ_a are 2.5, 2.6, and 7.7 at 1200 K, 770 K, and 77 K, respectively. Since ρ_c and ρ_a nearly satisfy the linear relationship of $\log \rho \propto T^{-1}$ for the higher temperature range, as shown in Fig. 4, they yield energy gap, E_g, values of 0.010(8) aJ (0.67(3) eV) and 0.011(5) aJ (0.72(0) eV), respectively.

The temperature dependence of thermoelectric power and Hall coefficient for the boule with Si/Mn atomic ratio of 1.72 are shown in Figs 5 and 6, respectively (as open points). As can be seen from the broken curves in Fig. 5, the curve of thermoelectric power of the boule in the c-axis direction, α_c, is similar to that in the a-axis direc-

TABLE II Resistivity, ρ, thermoelectric power α, and Hall coefficient, R, at room temperature measured for the middle portion of the $MnSi_{\sim 1.73}$ boules

Kinds of boule	ρ (10^{-5} Ω m)		α ($\mu V K^{-1}$)		R (10^{-9} $m^3 C^{-1}$)	
	ρ_c†	ρ_a	α_c	α_a	R_c	R_a
Si/Mn = 1.70*	5.38	1.10	129.0	91.0	2.6	3.2
Si/Mn = 1.72	5.48	1.08	125.0	94.2	2.5	3.1
Si/Mn = 1.75	5.52	1.12	127.5	93.0	2.4	3.0

*Si/Mn is nominal atomic ratio of silicon to manganese.
†Suffixes a and c show the values along a- and c-axis, respectively.

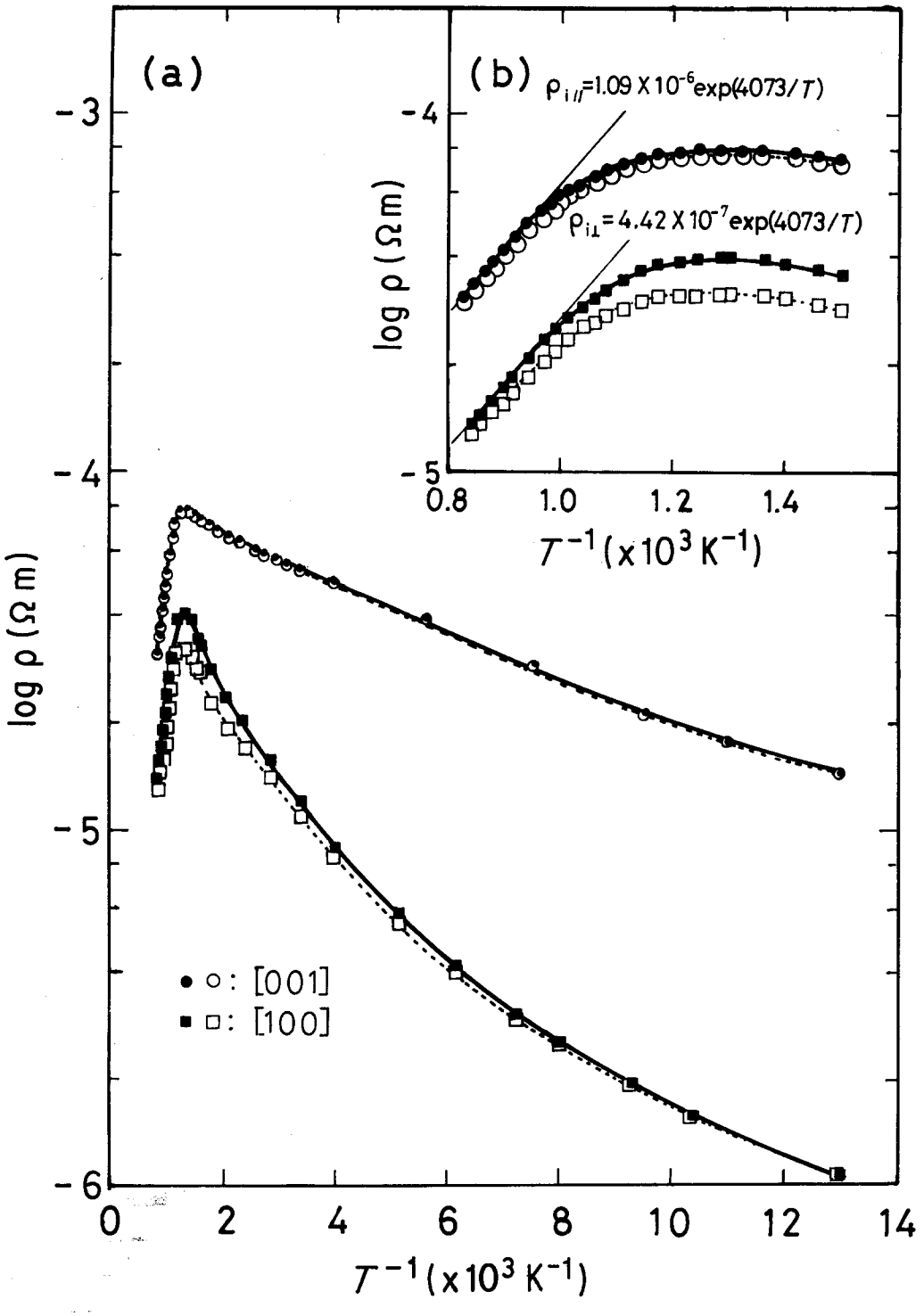

Figure 4 Temperature variations of resistivities for the boule with Si/Mn atomic ratio of 1.72 and for $Mn_{15}Si_{26}$. (a) for the whole temperature range; (b) for the temperature range near the intrinsic temperature region. Open and solid points show resistivities for the boule and for $Mn_{15}Si_{26}$, respectively. $\rho_{i\parallel}$ and $\rho_{i\perp}$ represent the intrinsic resistivities for $Mn_{15}Si_{26}$ in the [0 0 1] and [1 0 0] directions, respectively.

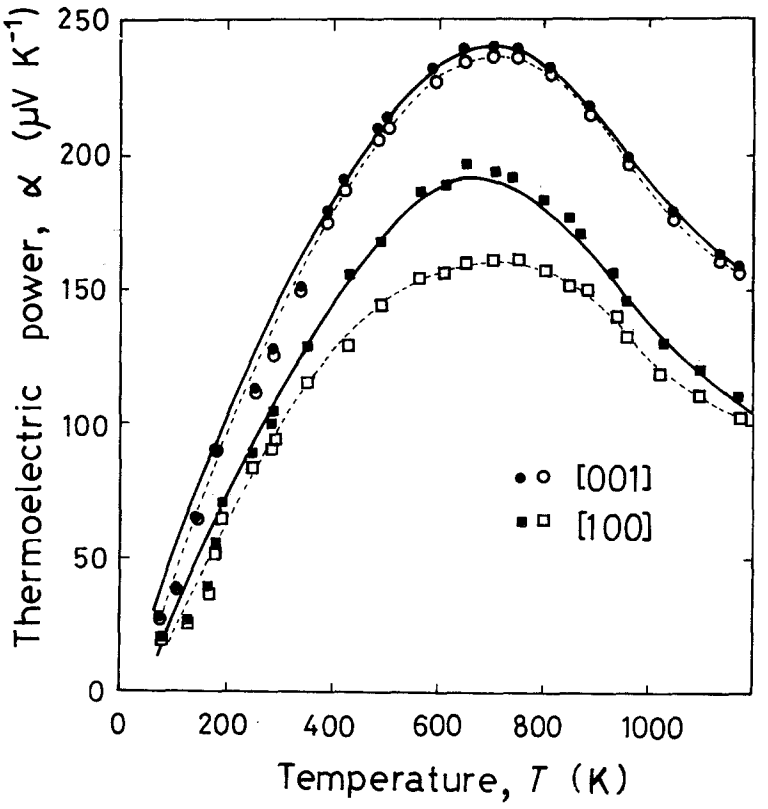

Figure 5 Temperature dependence of thermoelectric power for the boule with Si/Mn atomic ratio of 1.72 (open points) and for $Mn_{15}Si_{26}$ (solid points). Solid curves show the theoretical values.

tion, α_a; both curves have their maxima in the vicinity of 720 K. The ratio of α_c/α_a is about 1.5 and is independent of temperature over the whole temperature range. Hall coefficients in the c- and a-axis directions of the boule, R_c and R_a, respectively, decrease remarkably, with increasing temperature, above 650 K; temperature variations of R_c and R_a are slight below 650 K. The sign of R

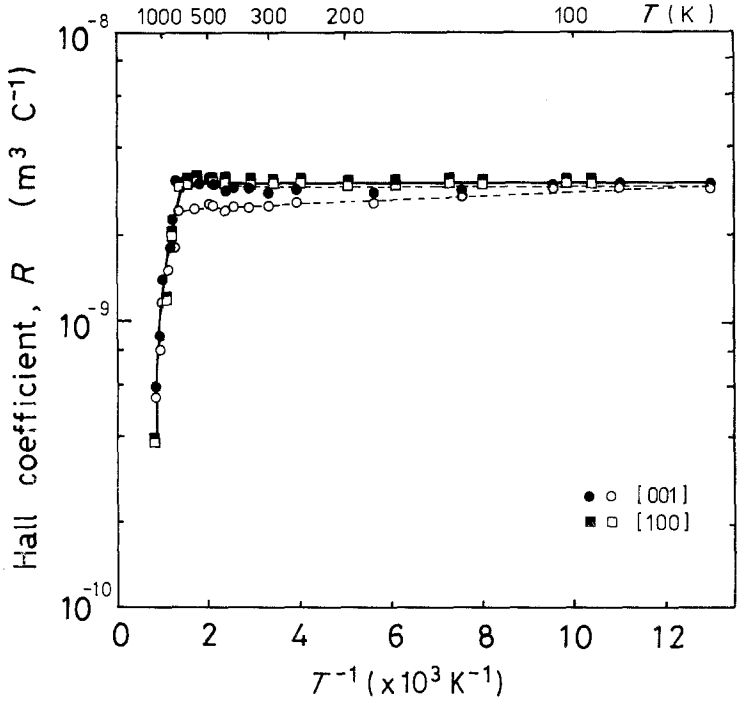

Figure 6 Temperature dependence of the Hall coefficient for the boule with Si/Mn atomic ratio of 1.72 (open points) and for $Mn_{15}Si_{26}$ (solid points).

is positive and corresponds with the sign of α over the whole temperature range. The ratio R_c/R_a is found to be smaller than unity as temperature increases, and Hall coefficient is anisotropic above 100 K; below this temperature, anisotropy is not recognizable within experimental error.

4. Discussion

4.1. Thermoelectric properties of $Mn_{15}Si_{26}$

The plate-like MnSi precipitates are distributed along the *c*-plane of the $Mn_{15}Si_{26}$ matrix in the Bridgman as-grown boules with Si-contents in the range from 63.0 to 63.6 at% and are stable even after annealing at 1373 K for 720 ksec. Since the existence of MnSi precipitates in the $MnSi_{\sim 1.73}$ boule has been reported by many investigators [19–24], it was considered that MnSi precipitates are inherent in the melt-grown boules, although such precipitates cannot be expected from the recent phase-diagram of the MnSi–Si system by Mager *et al.* [41].

On the other hand, MnSi has metallic properties [36, 37], and its resistivity, ρ_m, thermoelectric power, α_m, and Hall coefficient, R_m, have values much smaller than those of degenerate semiconducting $MnSi_{\sim 1.73}$ [27, 31, 32]. Additionally, since MnSi belongs to the cubic system $P2_13$–T^4 [1, 36] and since its thermoelectric properties are not practically anisotropic, the thermoelectric properties of the boule with MnSi-precipitates are considered to be smaller than those of the pure $Mn_{15}Si_{26}$ crystal. Then, thermoelectric properties of $Mn_{15}Si_{26}$ were evaluated from the model in which metallic MnSi and semiconducting $Mn_{15}Si_{26}$ are formed alternately in layers, as shown in Fig. 1, reported by Levinson [21].

From this model, the resistivity, $\rho_{\parallel}$, the thermoelectric power, $\alpha_{\parallel}$, and the Hall coefficient, $R_{\parallel}$, in the [0 0 1] direction of $Mn_{15}Si_{26}$ are described, respectively, as follows:

$$\rho_{\parallel} = (\rho_c - f\rho_m)/(1-f); \quad (1)$$

$$\alpha_{\parallel} = (\alpha_c - f\alpha_m)/(1-f); \quad (2)$$

$$R_{\parallel} = \left\{R_c - \frac{R_m}{1+\rho_m(1-f)/f\rho_{\perp}}\right\} \times \{1 + f\rho_{\perp}/\rho_m(1-f)\}, \quad (3)$$

where f is the volume-ratio of MnSi in the boule. Also, the resistivity, $\rho_{\perp}$, the thermoelectric power, $\alpha_{\perp}$, and the Hall coefficient, $R_{\perp}$, in the [1 0 0] direction of $Mn_{15}Si_{26}$ are represented by

$$\rho_{\perp} = \rho_a\rho_m(1-f)/(\rho_m - f\rho_a); \quad (4)$$

$$\alpha_{\perp} = \frac{f\rho_{\perp}(\alpha_a - \alpha_m) + \alpha_a\rho_m(1-f)}{\rho_m(1-f)}; \quad (5)$$

and

$$R_{\perp} = \frac{R_aR_m\{1 + \rho_{\parallel}(1-f)/f\rho_m\}}{\{1 + f\rho_m/\rho_{\parallel}(1-f)\}\{R_m\rho_{\parallel}(1-f)/f\rho_m - (R_a - R_m)\}}, \quad (6)$$

respectively. The effect of the interface between the MnSi and $Mn_{15}Si_{26}$ layers is ignored in these expressions because a three-dimensional transition-metal silicide has low mobility and so is predicted to show no practical boundary effects [19, 20, 26–29, 37]. Using values of ρ_m, α_m and R_m obtained at various temperatures, as reported by Gel'd *et al.* [36], the ρ, α, and R values for $Mn_{15}Si_{26}$ obtained from Equations 1 and 6 are plotted in Figs 4 to 6 (solid points) respectively.

As shown in Figs 4 to 6, the plots above 100 K are larger than those experimentally observed for the boule (broken lines), thus indicating that thermoelectric properties measured for the boule are smaller than the values for $Mn_{15}Si_{26}$. The fact that the $\rho_{\perp}$ and $\alpha_{\perp}$ values of $Mn_{15}Si_{26}$ are 28% larger than those of the boule, while the $\rho_{\parallel}$ and $\alpha_{\parallel}$ values are larger by only 2%, at 700 K indicates that the resistivities and thermoelectric powers of $Mn_{15}Si_{26}$ in the [1 0 0] direction are not practically influenced by the metallic MnSi. In the intrinsic temperature region, (as shown by solid lines in Fig. 4) temperature variations of $\rho_{\parallel}$ and $\rho_{\perp}$ behave as two linear functions, with the same gradient, according to the expression $\log\rho \propto T^{-1}$. The E_g value of $Mn_{15}Si_{26}$ obtained from these functions is 0.0112 ± 0.0001 aJ (0.702 ± 0.005 eV). Consequently, the intrinsic resistivities of $Mn_{15}Si_{26}$ in [0 0 1] $\rho_{i\parallel}$ and [1 0 0] $\rho_{i\perp}$ directions are expressed by

$$\rho_{i\parallel} = 1.09 \times 10^{-6} \exp(4073/T) \quad (7)$$

and

$$\rho_{i\perp} = 4.42 \times 10^{-7} \exp(4073/T), \quad (8)$$

expressed in Ω m, respectively.

As shown in Fig. 6, $R_{\parallel}$ and $R_{\perp}$ values for $Mn_{15}Si_{26}$ are in good agreement with each other over the whole temperature range and are in-

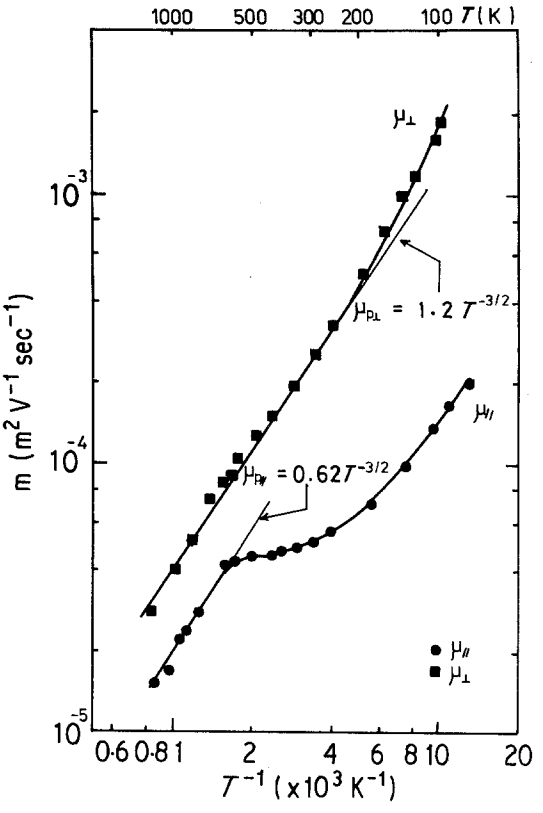

Figure 7 Hall mobilities of $Mn_{15}Si_{26}$ in the [0 0 1] and [1 0 0] directions. $\mu_{p\parallel}$ and $\mu_{p\perp}$ indicate hole mobilities in the [0 0 1] and [1 0 0] directions, respectively.

dependent of temperature below 670 K. The degenerate hole concentration, n_s, of $Mn_{15}Si_{26}$ is $2.1 \times 10^{27}\ m^{-3}$, indicating that $Mn_{15}Si_{26}$ is a degenerate p-type semi-conductor, where holes are highly degenerate as compared with those in stoichiometric $CrSi_2$ [39, 41–44] having $n_s = (4.2\text{–}5.2) \times 10^{26}\ m^{-3}$. The E_g value of $Mn_{15}Si_{26}$, evaluated from the relationship $\log (RT^{3/2}) \propto T^{-1}$ above 900 K, is 0.011 aJ (0.70 eV) and is in good agreement with the value obtained from ρ-data of $Mn_{15}Si_{26}$.

Fig. 7 shows the Hall mobilities of $Mn_{15}Si_{26}$ in [0 0 1] and [1 0 0] directions, $\mu_\parallel = R_\parallel/\rho_\parallel$ and $\mu_\perp = R_\perp/\rho_\perp$, as a function of reciprocal temperature. $\mu_\parallel$ and $\mu_\perp$ decrease with increasing temperature and obey a $T^{-3/2}$-law above 600 K and above 200 K, respectively. In these temperature ranges, as shown in Fig. 7, it is found that acoustic lattice scattering is dominant. Then the hole mobilities of $Mn_{15}Si_{26}$ in the [0 0 1] $\mu_{p\parallel}$ and [1 0 0] $\mu_{p\perp}$ directions are represented by

$$\mu_{p\parallel} = 0.62T^{-3/2} \tag{9}$$

and

$$\mu_{p\perp} = 1.2T^{-3/2}, \tag{10}$$

expressed in $m^2\,V^{-1}\,sec^{-1}$, respectively.

4.2. Carrier concentration of $Mn_{15}Si_{26}$

The electron-to-hole mobility ratio, b, which is necessary to evaluate the temperature variation of carrier concentration in $Mn_{15}Si_{26}$, was determined by using the method described by Hunter [46], in which b was estimated from the temperature dependence of resistivity between the extrinsic and the intrinsic regions. b values obtained from $\rho_\parallel$ and from $\rho_\perp$ measurements shown in Fig. 4 are 0.023 and 0.017, respectively, and the average value is in good agreement with $b = 0.02$ given by Nishida [32] for $MnSi_{\sim 1.73}$ alloys. Electron concentration, n, hole concentration, p, and R in the p-type semi-conductor are described by

$$n = p - n_s; \tag{11}$$

$$p = \left(\frac{1}{e\rho\mu_p} + bn_s\right) \Big/ (b+1), \tag{12}$$

and

$$R = \frac{p - nb^2}{e(nb+p)^2}, \tag{13}$$

respectively [47], where e is the elementary electron charge. Using the experimental values for $n_s = 2.1 \times 10^{27}\ m^{-3}$ and $b = 0.02$, values of p and n for $Mn_{15}Si_{26}$ are determined at various temperatures from Equations 9 to 12. The results are shown in Fig. 8 (solid curves) indicating that the theoretical curves fit the evaluated carrier concentrations of $Mn_{15}Si_{26}$. Hall coefficients in the vicinity of the intrinsic region are calculated from Equation 13 by using the calculated carrier concentrations. These are tabulated in Table III. Since $Mn_{15}Si_{26}$ is a highly degenerate semiconductor, as shown by Fig. 8, n is equal to p above 1000 K, indicating that the intrinsic conduction of $Mn_{15}Si_{26}$ appears in the extremely-high temperature range. The results further explain why the temperature variation of resistivity for $Mn_{15}Si_{26}$ obeys a $\log \rho \propto T^{-1}$ relation above 1000 K.

4.3. Thermoelectric power of $Mn_{15}Si_{26}$

As shown in Fig. 6, the thermoelectric power, α, for $Mn_{15}Si_{26}$ remains large and positive even at temperatures above 1000 K, where the concentrations of electrons and holes are taken to be comparable. This fact suggests that the hole

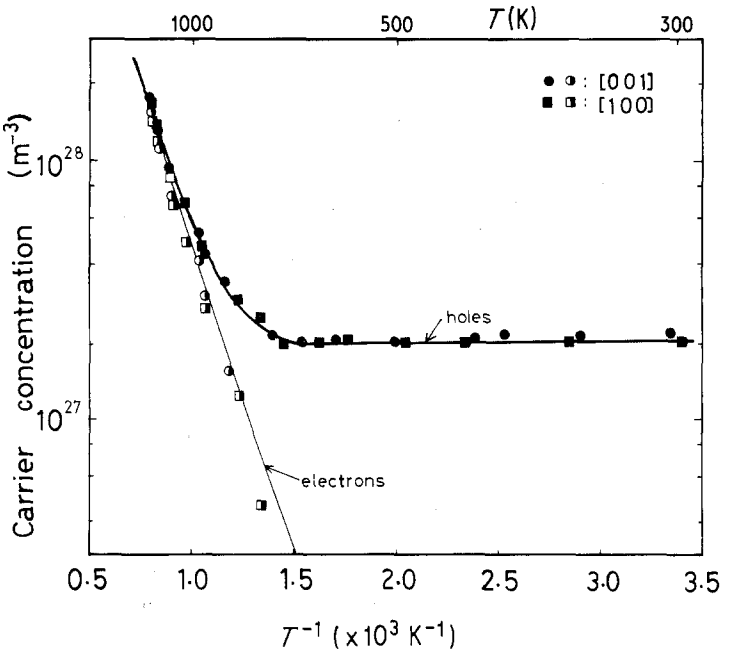

Figure 8 Carrier concentrations of holes and electrons for $Mn_{15}Si_{26}$ in the [0 0 1] and [1 0 0] directions. Solid curves show the theoretical values.

mobility is much larger than the electron mobility, and thus α, in the intrinsic region, is dominated by the more mobile holes. In order to analyse the temperature variation of thermoelectric power for $Mn_{15}Si_{26}$, the general expression, given by Ioffe [48], is used

$$\alpha = \pm \frac{k}{e}\left[\frac{\int_0^\infty \frac{df_0(\epsilon^*)}{d(\epsilon^*)} l(\epsilon^*)\epsilon^{*2}\, d\epsilon^*}{\int_0^\infty \frac{df_0(\epsilon^*)}{d(\epsilon^*)} l(\epsilon^*)\epsilon^*\, d\epsilon^*} - \mu^*\right], \quad (14)$$

where ϵ^* is kinetic energy of the carrier in kT units, $f_0(\epsilon^*)$ is the thermal equilibrium distribution function, $l(\epsilon^*)$ is the mean free path of the carriers, $\mu^* = \mu/kT$ is the reduced chemical potential and k is the Boltzmann constant. Plus and minus signs correspond to holes and electrons, respectively. Assuming that acoustic lattice scattering is dominant, as described in Section 4.1, and that $f_0(\epsilon^*)$ obeys Fermi–Dirac statistics ($Mn_{15}Si_{26}$ is a degenerate semi-conductor) Equation 14 can be rewritten as

$$\alpha = \pm \frac{k}{e}\left\{2\frac{F_1(\eta^*)}{F_0(\eta^*)} - \eta^*\right\}, \quad (15)$$

where F_1 is derived from the Fermi–Dirac integral by putting r = 1, and

$$F_r(\eta^*) = \int_0^\infty \frac{\epsilon^{*r}\, d\epsilon^*}{\exp(\epsilon^* - \eta^*) - 1}$$

is the well-known Fermi–Dirac integral [49] and η^* is the reduced Fermi energy of either holes or electrons. On the other hand, the hole concentration, p, is given by the following expression [48], when a parabollic structure is assumed for the region near the top of the valence band:

TABLE III Hall coefficient, R, and concentrations of electrons, n, and holes, p, for $Mn_{15}Si_{26}$ in the [0 0 1] and [1 0 0] directions, near the intrinsic conduction region

Crystal axis	Temperature, T (K)	Concentration (10^{27} m^{-3})		Hall coefficient (10^{-9} m^3 C^{-1})	
		p	n	R_{obs}	R_{cal}
[0 0 1]	1128	9.39	7.31	0.59	0.645
	1040	6.14	4.06	0.88	0.990
	964	4.03	1.96	1.4	1.52
[1 0 0]	1219	17.3	15.2	0.30	0.349
	1174	13.3	11.2	0.38	0.454
	1020	6.92	4.84	0.88	0.878
	952	4.71	2.63	1.2	1.30

$$p = \frac{4\pi(2m_p^* kT)^{3/2}}{h^3} F_{1/2}(\eta_p^*), \qquad (16)$$

where h is Plank's constant, m_p^* is the hole effective mass, and η_p^* is the reduced Fermi energy of the holes.

As mentioned in Section 4.1, $\mu_{p\parallel}$ and $\mu_{p\perp}$ values for $Mn_{15}Si_{26}$ in the degenerate state obey a $T^{-3/2}$-law in the temperature regions from 600 to 700 K and from 200 to 700 K, respectively. Hole effective masses for $Mn_{15}Si_{26}$ in [0 0 1] $m_{p\parallel}^*$ and [1 0 0] $m_{p\perp}^*$ directions were then evaluated from Equations 15 and 16 by using values of $\alpha_\parallel$ and $\alpha_\perp$ in the vicinity of 600 K and $n_s = 2.1 \times 10^{27}$ m^{-3}. This gives $m_{p\parallel}^* = 15 m_0$ and $m_{p\perp}^* = 11 m_0$, where m_0 is the effective mass of a free electron.

Thermoelectric power in the intrinsic region is given by

$$\alpha = \rho\{(\alpha_p/\rho_p) + (\alpha_n/\rho_n)\}, \qquad (17)$$

where the suffixes p and n refer to holes and electrons, respectively. Using the relation $(\eta_p^* + \eta_n^*) = -E_g/kT$, where η_n^* is the reduced Fermi energy of electrons, Equation 17 is reduced to

$$\alpha = \frac{k}{e}\left[\frac{2p}{(nb+p)}\frac{F_1(\eta_p^*)}{F_0(\eta_p^*)} - \frac{nb}{nb+p} \times \left\{2\frac{F_1(-\eta_p^* - E_g^*)}{F_0(-\eta_p^* - E_g^*)} + E_g^*\right\} - \eta_p^*\right], \qquad (18)$$

where $E_g^* = E_g/kT$. Putting $m_{p\parallel}^* = 15 m_0$ and using the calculated values of p and n at various temperatures, the values of η_p^* were estimated from Equation 16, and these values were then used in Equation 18 to calculate the temperature variation of $\alpha_\parallel$. The experimentally determined values of $b = 0.02$ and $E_g = 0.0112$ aJ (0.702 eV) were also used in the calculations. The same calculations were carried out for $\alpha_\perp$ using $m_{p\perp}^* = 11 m_0$. These results are shown by the solid curves in Fig. 5. Plots of $\alpha_\parallel$ and $\alpha_\perp$ in Fig. 5 shown as solid marks fit the theoretical curves above 400 and 200 K, respectively. In the lower temperature range, the values of $\alpha_\parallel$ and $\alpha_\perp$ shift to values larger than the theoretically calculated values because acoustic lattice scattering is no longer the dominant scattering mechanism, as shown in Fig. 7. The scattering mechanism of carriers at low temperatures is not clear at the present time.

5. Conclusions

Boules in which the atomic composition ratios of silicon to manganese are 1.70, 172, and 1.75 were grown by the Bridgman method, in order to investigate crystalline and thermoelectric properties for the most silicon-rich silicide of manganese. In all the boules, except in the upper and lower ends of some boules, it was found that plate-like MnSi precipitates were distributed along the c-plane of $Mn_{15}Si_{26}$ matrix and remained stable after annealing at 1373 K for 720 ksec, and that the volume-ratio of MnSi to $Mn_{15}Si_{26}$ was 0.02. Using this ratio, the Si-content of the boule was evaluated to be 63.1(7) at% ($MnSi_{1.715}$), a value in reasonable agreement with the value determined by chemical analysis.

In order to analyse the semiconducting behaviour of $Mn_{15}Si_{26}$, the electrical resistivities, Hall coefficients, and thermoelectric powers of the boules in the [0 0 1] and [1 0 0] directions were measured over the temperature range from 77 to 1200 K. On the basis of the distribution state of MnSi precipitates in the boules, thermoelectric properties of $Mn_{15}Si_{26}$ were estimated using the assumption that metallic MnSi and semiconducting $Mn_{15}Si_{26}$ were formed in alternate layers. It was found that resistivities and thermoelectric powers in the [0 0 1] and [1 0 0] directions of $Mn_{15}Si_{26}$ show an anisotropy, although the Hall coefficient is isotropic over the whole temperature range. Hole effective masses of $Mn_{15}Si_{26}$ in the [0 0 1] and [1 0 0] directions were found to be 15 and 11 times as large as the free electron mass, respectively. Putting $m_{p\parallel}^* = 15 m_0$ and $m_{p\perp}^* = 11 m_0$, the calculated thermo-electric powers in the [0 0 1] and [1 0 0] directions were in reasonable agreement with those powers estimated for $Mn_{15}Si_{26}$ above 400 and above 200 K, respectively.

References

1. R. KIEFFER, F. BENESOVSKY and E. HONAK, *Z. Anorg. Allg. Chem.* **268** (1951) 191.
2. R. KIEFFER, F. BENESOVSKY and C. KONOPIKY, *Ber. Deut. Keram. Ges.* **31** (1954) 223.
3. A. W. SEARCY, *J. Amer. Ceram. Soc.* **40** (1957) 417.
4. P. V. GEL'D, *Zh. Tekh. Fiz.* **27** (1957) 113.
5. E. N. NIKITIN, *ibid.* **28** (1958) 23, 26.
6. V. S. NESHPOR and V. I. YUPKO, *Poroshkovaya Metallurgiya* **3** (1963) 55.
7. B. BOREN, *Arkiv Kemi. Min. Geol.* **11A** (1933) 1.
8. M. HANSEN, "Constitution of Binary Alloys" (McGraw-Hill Book Co., New York, 1959) p. 953.
9. V. A. KORSHUNOV, F. A. SIDORENKO, P. V. GEL'D and K. H. DAVYDOV, *Fiz. Metal. Metalloved.* **12** (1961) 277.
10. L. D. DUDKIN and E. S. KUZNETSOVA, *Poroshkovaya Metallurgiya* **1** (1962) 20.

11. O. SCHWOMMA, H. NOWOTNY and A. WITTMAN, *Monatsh. Chem.* **94** (1963) 681.
12. Y. FUJINO, D. SHINODA, S. ASANABE and Y. SASAKI, *Jap. J. Appl. Phys.* **3** (1964) 431.
13. F. LAVES and H. J. WALLBAUM, *Z. Kristallogr.* **A101** (1939) 78.
14. O. SCHWOMMA, A. PREISINGER, H. NOWOTNY and A. WITTMAN, *Monatsh. Chem.* **95** (1965) 1527.
15. A. BOREN, "Borides, Silicides and Phosphides" edited by B. Aronsson, R. Lundslrom and S. Rundquist (Methuen and Co., London and New York, 1965).
16. H. W. KNOTT, M. H. MUELLER and L. HEATON, *Acta Cryst.* **23** (1967) 549.
17. G. ZWILLING and H. NOWOTNY, *Monatsh. Chem.* **102** (1971) 672.
18. O. G. KARPINSKII and B. A. EVSEEV, *Izd. Akad. Nauk SSSR, Neorg. Materialy* **5** (1969) 525.
19. L. D. IVANOVA, N. KH. ABRIKOSOVA, E. I. ELAGINA and V. D. KHVOSTIKOVA, *ibid.* **5** (1969) 1933.
20. N. KH. ABRIKOSOVA and L. D. IVANOVA, *ibid.* **10** (1974) 1016.
21. L. M. LEVINSON, General Electric Technical Information Series Number 72CRD111, March, 1972, p. 1.
22. T. KOJIMA and I. NISHIDA, *Jap. J. Appl. Phys.* **14** (1975) 141.
23. *Idem, J. Crystal Growth* **47** (1979) 589.
24. I. KAWASUMI, I. NISHIDA, K. MASUMOTO and M. SAKATA, *Jap. J. Appl. Phys.* **15** (1976) 1405.
25. V. A. KORSHUNOV and P. V. GEL'D, *Fiz. Metal. Metalloved.* **11** (1961) 945.
26. D. SHINODA and S. ASANABE, *J. Phys. Soc. Jap.* **21** (1966) 555.
27. W. B. BIENERT and E. A. STRABEK, Proceedings of the IEEE/AIAA Thermoelectric Specialists Conference (Institute of Electrical and Electronics Engineers, New York, 1966) p. 10.
28. B. K. VORONOV, L. D. DUDKIN and N. N. TRUSOVA, *Kristallografiya* **12** (1967) 519.
29. E. N. NIKITIN, V. I. TARASOV, A. A. ANDREEV and L. N. SHUMILOVA, *Fiz. Tverd. Tela* **11** (1969) 2389.
30. E. N. NIKITIN, V. I. TARASOV and P. V. TMARIN, *ibid.* **11** (1969) 234.
31. E. N. NIKITIN and V. I. TARASOV, *ibid.* **13** (1971) 2938.
32. I. NISHIDA, *J. Mater. Sci.* **7** (1972) 435.
33. E. N. NIKITIN, V. I. TARASOV and V. K. ZAITSEV, *Fiz. Tverd. Tela* **15** (1973) 1254.
34. V. K. ZAITSEV, V. I. TARASOV and A. A. ADILBEKOV, *ibid.* **17** (1975) 581.
35. V. I. TARASOV, E. N. NIKITIN and L. N. SHUMILOVA, *Izd. Akad. Nauk SSSR, Neorg. Materialy* **11** (1975) 1038.
36. P. V. GEL'D and F. A. SIDORENKO, "Silitsid Perekhodnikh Metallov Chetvertogo Perioda (English title: Transition Metal Silicides of the Fourth Period) (Metallurgiya, Moskva, 1971) p. 365, 497.
37. S. ASANABE, *J. Phys. Soc. Jap.* **20** (1965) 933.
38. T. SAKURAI, "Crystal Structure Analysis II" (Crysallographic Society of Japan, Tokyo, 1967) p. 99.
39. E. H. PUTLEY, "The Hall Effect and Related Phenomena" (Butterworth and Co., London, 1960) p. 61.
40. T. SAKATA and T. TOKUSHIMA, *Trans. Nat. Res. Inst. Metals* **5** (1963) 34.
41. T. MAGER and E. WACHTEL, *Z. Metallkde.* **61** (1970) 853.
42. D. SHINODA, S. ASANABE and Y. SASAKI, *J. Phys. Soc. Jap.* **19** (1964) 269.
43. I. A. SALTYKOVA, KH. GOL'DBERG, F. A. SIDORENKO and P. V. GEL'D, *Poroshkovaya Metallurgiya* **66** (1968) 73.
44. I. NISHIDA, *J. Mater. Sci.* **7** (1972) 1119.
45. E. N. NIKITIN, V. I. TARASOV and V. K. ZAITSEV, *Fiz. Tverd. Tela* **15** (1973) 1254.
46. L. P. HUNTER, *Phys. Rev.* **91** (1953) 579.
47. G. L. PEARSON and J. BARDEEN, *ibid.* **75** (1949) 865.
48. A. F. IOFFE, "Physics of Semiconductors", translated by H. J. Goldsmid (Infosearch, London, 1960) p. 305.
49. J. McDAUGALL and E. G. STONER, *Phil. Trans.* **A237** (1938) 67.

Received 8 May and accepted 1 July 1980.